

Fig. 1. Sparsity pattern of the Exciton200 (left panel, dimension  $D = 193\,443\,603$ ) and Hubbard16 (right panel, dimension  $D = 165\,636\,900$ ) matrices from the scalable matrix collection ScaMaC [1].

some applications remains a computational challenge [25, 29, 35, 38]. In this context, techniques such as subspace iteration or filter diagonalization (FD) have resurfaced [16, 28, 30, 44, 45] as an alternative to the Lanczos or Jacobi-Davidson algorithms [8, 12, 32, 39].

Efficient, cost-effective computations require good algorithms and performant implementations. For the parallelized solution of large-scale eigenvalue problems the main issues are the performance and the parallel efficiency of the two central operations, sparse matrix-vector multiplication (SpMV) and orthogonalization. Beyond the ubiquitous memory bandwidth bottleneck, the main limiting factor is communication among processes. While communication-avoiding techniques exist for orthogonalization [11, 41], communication cannot be avoided in distributed SpMV.

The significance of communication, mainly quantified by the communication volume per SpMV, depends on the sparsity pattern of the matrix. Two typical matrices from quantum physics applications [2–4, 9] are shown in Fig. 1. For the “tame” sparsity pattern of the Exciton200 matrix we expect that communication is insignificant and can overlap with computation and local memory access. For the “rugged” sparsity pattern of the Hubbard16 matrix we expect that communication dominates the SpMV to such an extent that scalability and parallel efficiency are lost. We will later be able to differentiate these cases with a communication metric (see Sec. 3.1).

In the present paper we describe how scalability and parallel efficiency can be restored if one recognizes that an eigensolver such as FD, and in fact any block eigensolver with multiple search vectors, possesses two orthogonal layers of parallelism: a “horizontal layer,” where each vector is distributed across multiple processes, and a “vertical layer,” where bundles of vectors are distributed across different process groups. The two layers allow us to choose and compare different layouts of the distributed vectors.

Making use of the two layers of parallelism is not an entirely trivial task since SpMV and orthogonalization have competing communication patterns: Distributed vector layouts that are optimal for SpMV do not coincide with those optimal for orthogonalization. The first objective of the present paper is, therefore, to introduce communication metrics that quantify the trade-off between communication during SpMV and during redistribution of vectors between different layouts. The second objective is to validate our communication metrics with extensive benchmarks for real application matrices, such as those depicted in Fig. 1. The third objective is to study the performance benefits of using the two layers of parallelism in large-scale eigenvalue computations, here with the FD scheme.

Note that the present paper has no intention to address algorithmic issues of FD. We use FD as an example of an eigensolver that allows us to reliably compute several or many eigenvalues even for complicated matrices and to apply our analysis of communication in SpMV in a relevant computational context. While FD provides the present computational context, our performance

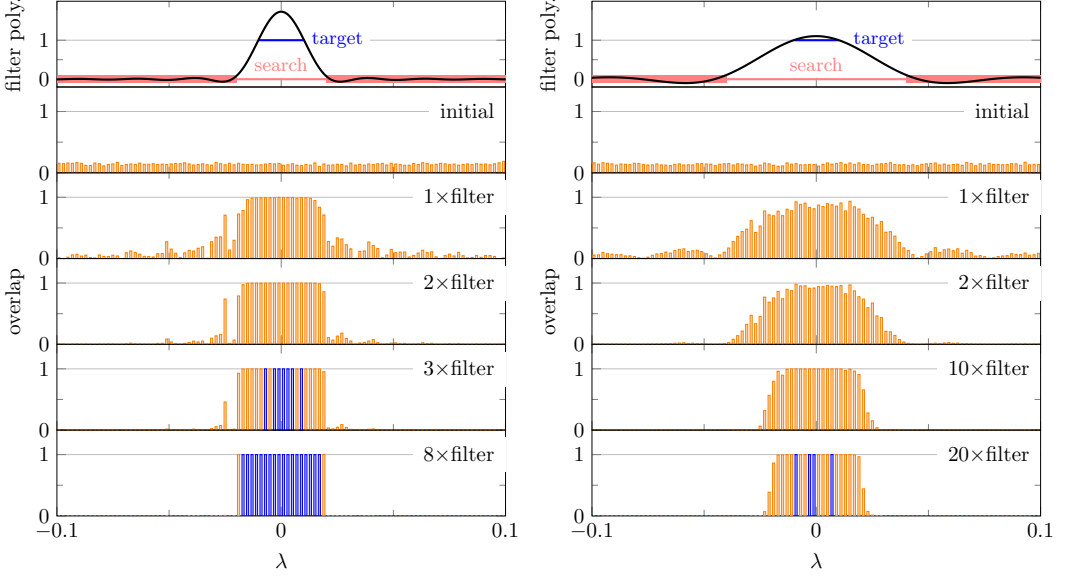


Fig. 2. Filter diagonalization for 1000 equidistant eigenvalues in the interval  $[-1, 1]$ . The top panels show the filter polynomial for target interval  $[-0.01, 0.01]$  (with  $N_t = 10$ ) and search interval  $[-0.02, 0.02]$  (left column) or  $[-0.04, 0.04]$  (right column). Outside of the search interval the filter polynomial is small, as indicated by the red boxes which contain the polynomial. The lower panels show the overlap of the search space (with  $N_s = 20$  vectors) with the true eigenvectors. In the left column, where the search interval contains less than  $N_s$  eigenvalues, filter diagonalization converges with eight applications of the polynomial filter (converged vectors with overlap above  $1 - \epsilon$ , for  $\epsilon = 10^{-7}$ , are shown in blue; converged eigenvalues cover the target interval and may extend into the search interval). In the right column, where the search interval contains more than  $N_s$  eigenvalues, filter diagonalization does not converge.

analysis in terms of the communication metrics is not restricted to FD but extends to any block eigensolver where SpMV applied to multiple vectors is a dominant operation. Therefore, we restrict ourselves to the plain FD scheme, even though we are aware that it will not serve as a general-purpose eigensolver, and postpone algorithmic considerations to future work.

The paper is organized from this viewpoint. In Sec. 2 we recall the basics of FD in the context of large-scale computations. In Sec. 3 we describe the two orthogonal layers of parallelism and introduce the communication metrics that are pivotal to our performance analysis. We use the communication metrics to analyze a number of SpMV benchmarks. Then, we discuss how different vector layouts allow us to restore scalability and parallel efficiency of SpMV. In Sec. 4 we validate this approach using FD for the solution of large-scale eigenvalue problems in the exciton and Hubbard application cases. Finally, we summarize in Sec. 5. The appendix provides further benchmarks for various other application matrices.

## 2 OUTLINE OF FILTER DIAGONALIZATION

FD proceeds by repeated application of a (polynomial) filter to a search space of  $N_s$  independent vectors. Each application of the filter amplifies (suppresses) targeted (unwanted) eigenvectors of a given matrix  $\hat{A}$ , until a subset of  $N_t$  vectors has converged to the eigenvectors corresponding to the eigenvalues closest to a target  $\tau$ . This scheme is illustrated in Fig. 2.

---

**Algorithm 1** Outline of a minimal FD algorithm, with redistribution of vectors between the stack layout and the panel layout in steps 7, 9.

---

```

1:      compute spectral inclusion interval  $[\lambda_l, \lambda_r]$  ▷ with Lanczos
2:       $V \leftarrow N_s$  random search vectors
      repeat
3:           $V \leftarrow \text{orthogonalize}[V]$  ▷ in stack layout
4:          if ( $\geq N_t$  converged Ritz vectors  $\in V$ ): exit iteration
5:          compute search & target interval
6:          construct filter polynomial  $p(\cdot)$ 
            $\lceil \text{stack} \rightarrow \text{panel layout}$ 
7:          if  $N_{\text{col}} > 1$ :
               redistribute vectors  $V$  from stack to panel layout
8:           $V \leftarrow p[\hat{A}]V$  ▷ in  $N_{\text{row}} \times N_{\text{col}}$  panel layout
9:          if  $N_{\text{col}} > 1$ :
               redistribute vectors  $V$  from panel to stack layout
            $\lceil \text{stack} \leftarrow \text{panel layout}$ 
10:     end repeat

```

---

For large-scale problems, where matrix inversion or factorization [7, 31] is not an option, the restriction to polynomial filters is unavoidable. A polynomial filter maps search vectors  $v \mapsto p[\hat{A}]v$ , where the filter polynomial  $p(\cdot)$  is constructed to be large (small) inside (outside) of a target interval around the target  $\tau$ . Since  $p[\hat{A}]$  is a polynomial in the matrix  $\hat{A}$  it can be evaluated with SpMV.

FD works equally for extremal and interior eigenvalues, although convergence for extremal eigenvalues is considerably faster than for interior eigenvalues [28, 34]. The large-scale computations considered here, where the target interval is a small fraction of the entire spectrum, easily require a polynomial degree of order  $10^3$  or higher.

Convergence of FD depends not only on the quality of the filter polynomial but also on the number of search vectors  $N_s$ . For fast convergence one should choose  $N_s \gg N_t$ . Often,  $N_s/N_t \simeq 4$  is a reasonable choice (see [28] for an extended analysis). Therefore, for a  $D$ -dimensional eigenproblem, the effective problem size in FD is  $D \times N_t$  if  $N_t \geq 1$  eigenvectors are requested, and the effective computational size is  $D \times N_s$  instead of just  $D$ . As discussed in Sec. 3, this allows us to parallelize the problem both along the “vertical” axis  $D$  and the “horizontal” axis  $N_s$ , which results in two orthogonal layers of parallelism.

Note that we do not split the problem into multiple independent (“embarrassingly parallel”) computations with a smaller number of target and search vectors, as would be done in a “spectrum slicing” approach [24]. An essential lesson from the analysis in, e.g., Ref. [28] is that a reduction of the size of the search space is paid for with a disproportionate increase in the degree of the filter polynomial, and hence of the total computational effort. Convergence of FD for large-scale problems calls for a large search space.

Starting from the illustration of the FD scheme in Fig. 2 we arrive at Algorithm 1. The algorithm already contains steps 7 and 9 associated with the two layers of parallelism that will be discussed in Sec. 3. Apart from these steps, the algorithm comprises only standard operations.

The preparatory phase (steps 1, 2) computes (using, e.g., a few steps of the Lanczos algorithm) a spectral inclusion interval  $[\lambda_l, \lambda_r]$  that is required for the polynomial filter in Chebyshev form [43]. The FD iteration alternates between orthogonalization (step 3) and the polynomial filter (step 8). The algorithm terminates successfully when  $N_t$  eigenvectors with eigenvalues in the target interval

**Algorithm 2** Evaluation of the polynomial filter  $V \mapsto p[\hat{A}]V$  for a filter polynomial  $p(x) = \sum_{k=0}^n \mu_k T_k(x)$ , given as a Chebyshev expansion of degree  $n \geq 2$ . The algorithm requires two matrices  $W_1, W_2$  with the same size as  $V$  as workspace for the Chebyshev iteration. The scaling parameters  $\alpha, \beta$  are determined from the spectral inclusion interval  $[\lambda_l, \lambda_r]$ . The SpMV and axpy operations in step 7 are fused into a single compute kernel to avoid reloading  $W_2$  from memory [19].

---

1:	$\alpha \leftarrow 2/(\lambda_r - \lambda_l), \quad \beta \leftarrow (\lambda_l + \lambda_r)/(\lambda_l - \lambda_r)$	
2:	$W_1 \leftarrow \alpha \hat{A}V + \beta V$	▷ SpMV
3:	$W_2 \leftarrow 2\alpha \hat{A}W_1 + 2\beta W_1 - V$	▷ SpMV
4:	$V \leftarrow \mu_0 V + \mu_1 W_1 + \mu_2 W_2$	
5:	<b>for</b> $k = 3$ to $n$ <b>do</b>	
6:	$(W_1, W_2) \leftarrow (W_2, W_1)$	▷ swap pointers
7:	$W_2 \leftarrow 2\alpha \hat{A}W_1 + 2\beta W_1 - W_2$	▷ SpMV
	$V \leftarrow V + \mu_k W_2$	& BLAS axpy
8:	<b>end do</b>	

---

have converged. To detect this, we measure the residual  $\rho = \|\hat{A}\vec{v} - \lambda\vec{v}\|_2$  of the current best  $N_t$  approximate Ritz vectors in the search space and demand  $\rho \leq 10^{-10}$  for convergence.

During the FD iteration the algorithm has to keep track of the target and search intervals  $[\tau_l, \tau_r]$  and  $[\sigma_l, \sigma_r]$ , which are not known in advance. The target (search) interval must contain at least  $N_t$  (at most  $N_s$ ) eigenvalues of  $\hat{A}$ . If the search interval is too large, FD fails to converge, as shown in the right column of Fig. 2; if it is too small, the required degree of the filter polynomial becomes unnecessarily high. Different strategies for the selection of the target and search intervals have a profound impact on the total number of FD iterations, which leaves much room for algorithmic optimization. Currently, we determine both intervals from Lehmann intervals [22].

For a given target and search interval, the filter polynomial is constructed from the Chebyshev expansion  $p(x) = \sum_{k=0}^n \mu_k T_k(x)$  of a window function (see Ref. [28] for definitions), or from a more general polynomial approximation [13, 33]. The evaluation of the polynomial filter  $V \mapsto p[\hat{A}]V$  uses the Chebyshev iteration in Algorithm 2. The polynomial filter is applied simultaneously to all search vectors, which are given as the columns of a  $D \times N_s$  matrix  $V$ . For polynomial degree  $n$ , the evaluation requires  $n$  SpMVs and BLAS level 1 vector-vector operations.

Note that the SpMVs in Algorithm 2 are executed simultaneously for multiple vectors  $V$  in the form of a “sparse matrix-multiple-vector multiplication,” which allows for extensive node-level performance engineering through the reduction of memory traffic [19]. Conversely, this implies that the communication overhead of distributed SpMV is the single limiting factor for scalability and parallel efficiency of the polynomial filter.

After the initial assignment of random vectors and after each application of the polynomial filter, the search vectors need to be orthogonalized. Afterwards, a single additional SpMV provides the Ritz values and Lehmann intervals used to check for convergence and to determine the current target and search interval. For orthogonalization, a communication-avoiding technique such as the SVQB method [41] or the tall skinny QR decomposition (TSQR) [11] should be used. We use TSQR because of its superior numerical stability for a large number of search vectors.

### 3 THE TWO ORTHOGONAL LAYERS OF PARALLELISM

The FD iteration alternates between two operations with competing communication patterns, the polynomial filter and orthogonalization. According to the discussion in Sec. 2, evaluation of the polynomial filter requires many SpMVs ( $\propto n$ ) for many vectors ( $\propto N_s$ ). For large problem sizes (vector dimension  $D \gtrsim 10^8$ , number of search vectors  $N_s > N_t \gtrsim 10$ ), FD cannot be executed on a

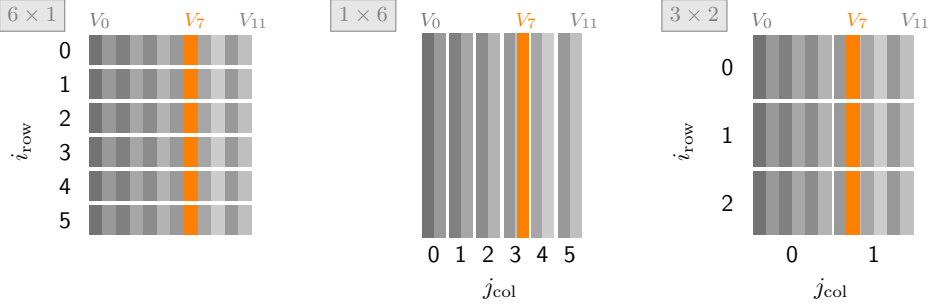


Fig. 3. Illustration of the (from left to right)  $6 \times 1$  panel = “stack”,  $1 \times 6$  panel = “pillar”, and  $3 \times 2$  panel layout for  $N_s = 12$  column vectors  $V_0, \dots, V_{11}$  distributed across  $\mathcal{P} = 6$  processes. Orthogonalization (or SpMV) requires communication of vector entries along the horizontal (or vertical) axis. This leads to two orthogonal layers of parallelism in the FD algorithm.

single compute node with limited memory resources but requires distributed computing. This is the setting for the performance analysis in the present section.

The key decision in distributed sparse linear algebra is how to distribute vectors and matrices across the parallel processes. Note that by “process” we will usually mean an MPI process in a hybrid MPI+X program (often, X=OpenMP). One MPI process may span an entire compute node or is associated with an individual non-uniform memory access (NUMA) locality domain. The basic assumption is that communication between different processes crosses node or NUMA boundaries and is significantly slower than shared-memory access within a single process.

Three different distributed vector layouts are depicted in Fig. 3, where the FD search vectors are assembled as the columns of a  $D \times N_s$  matrix  $V = (V_0, V_1, \dots, V_{N_s-1})$ . These vectors have to be distributed across  $\mathcal{P}$  processes, where  $\mathcal{P}$  denotes the total number of processes at our disposal.

In the standard “stack” layout as depicted in the left panel in Fig. 3, the  $N_s$  search vectors are sliced horizontally such that each of the  $\mathcal{P}$  processes keeps a fraction  $1/\mathcal{P}$  of every search vector, i.e.,  $D/\mathcal{P}$  rows of the matrix  $V$ . In this layout, orthogonalization requires minimal communication. For example, computation of the Gram matrix  $V^T V$  needed in SVQB orthogonalization [41] requires only communication of local scalar products in a global MPI\_Allreduce operation. The aggregated communication volume is of order  $\mathcal{P} \times N_s^2$  and independent of  $D$ . The TSQR scheme is more involved but still requires only minimal communication [11]. SpMV, on the other hand, needs to communicate the vector entries between processes. The communication volume depends on the sparsity pattern of the matrix at hand. Already visual inspection of Fig. 1 reveals that the communication volume of SpMV with the Hubbard matrix exceeds that with the stencil-like Exciton matrix. The difference is quantified by the  $\chi$  communication metrics introduced below.

In the alternative “pillar” layout shown in the central panel of Fig. 3, each process keeps a bundle of  $N_s/\mathcal{P}$  entire search vectors. Pictorially, we slice the matrix  $V$  of search vectors vertically instead of horizontally. In this layout, SpMV does not require any inter-process communication. Orthogonalization, however, now entails communication of entire vectors (e.g., to compute a scalar product). The minimal communication volume is of the order  $D \times N_s \times (1 - 1/\mathcal{P})$  vector entries, e.g., to assemble all vectors at one process, which likely exceeds that of SpMV in the stack layout.

The stack (with  $N_{\text{col}} = 1$ ) and pillar (with  $N_{\text{row}} = 1$ ) layout are special cases of the general “panel” vector layout depicted in the right panel of Fig. 3. For the panel layout, we arrange the  $\mathcal{P}$  processes as a rectangular  $N_{\text{row}} \times N_{\text{col}}$  Cartesian grid. We can freely vary the number of process rows and

columns to obtain differently shaped panel layouts, provided that the total number of processes  $\mathcal{P} = N_{\text{row}} \times N_{\text{col}}$ , which depends on the available compute resources, remains fixed.

Distribution of vectors according to the Cartesian grid of the panel layout introduces the two orthogonal (horizontal vs. vertical) layers of parallelism. Since orthogonalization requires communication along the horizontal axis and SpMV along the vertical axis of Fig. 3, the panel layout can achieve a trade-off between the competing communication patterns of orthogonalization and the polynomial filter in the FD iteration. Whether a trade-off is achieved and what speedup of the whole FD iteration can be expected with a panel layout depends on a number of parameters, including the  $\chi$  communication metric for SpMV introduced below.

Note that a panel layout of vectors or matrices is used in other contexts, e.g., in the block-cyclic data layout of ScaLAPACK [6]. In difference to ScaLAPACK, we here deal with sparse instead of dense linear algebra operations. Depending on the sparsity pattern, SpMV results in an irregular communication pattern that needs to be captured by the appropriate metrics. We also have to consider switching between different vector layouts to accommodate the competing communication patterns of SpMV and orthogonalization.

### 3.1 Communication metrics for distributed sparse matrix-vector multiplication

In distributed SpMV, a process evaluates the matrix-vector product  $y = \hat{A}x$  for several consecutive rows  $i \in [a:b]$ , as in the expression

$$y_i = \sum_{\substack{j=0 \\ A_{ij} \neq 0}}^{D-1} A_{ij}x_j \quad (\text{for } i \in [a:b]) . \quad (1)$$

Here,  $[a:b] = \{i \in \mathbb{Z} : a \leq i < b\}$  denotes the range of integers from  $a$  (included) to  $b$  (excluded) in slice notation. Note that we use zero-based indexing throughout this work. If the SpMV is distributed uniformly across  $N_p$  processes we have  $b - a \approx D/N_p$ .

During evaluation of Eq. (1),

$$n_m = |\{(i, j) : A_{ij} \neq 0 \text{ for } i \in [a:b], j \in [0:D]\}| \quad (2)$$

matrix elements are read from local memory. Here,  $|S|$  denotes the number of elements in the set  $S$ . Usually,  $n_m \approx (b - a)n_{\text{nzr}}$ , where  $n_{\text{nzr}}$  is the average number of non-zeros per matrix row.

Vector entries are distributed across the processes according to the distribution of the matrix rows. Therefore, a lower limit for the number of vector entries read from local memory during evaluation of Eq. (1) is given by

$$n_{\text{vm}} = |\{j : A_{ij} \neq 0 \text{ for } i, j \in [a:b]\}| . \quad (3)$$

In almost all situations, we have  $n_{\text{vm}} = b - a \approx D/N_p$ .

In FD, the SpMV is executed as a block operation on  $n_b$  vectors (where  $n_b \approx N_s/N_{\text{col}}$  in the panel layout). A lower limit for the data volume read from local memory (matrix elements and vector entries) thus is

$$V_m = n_m(S_d + S_i) + (b - a)S_i + n_b n_{\text{vm}} S_d , \quad (4)$$

where  $S_d$  (or  $S_i$ ) denotes the size of a single matrix/vector data (or matrix index) element in bytes. For a real (complex) matrix in double precision we have  $S_d = 8$  ( $S_d = 16$ ), and  $S_i = 4$  for uint32 indices for matrix dimensions  $D < 2^{32} \approx 4 \times 10^9$ . The second summand in Eq. (4) accounts for reading of the row pointers of a matrix stored in, e.g., Compressed Row Storage (CRS) format [5], and can often be neglected.

For optimal memory access patterns and cache reuse, the matrix of vectors  $V$  should be stored in row-major order [19]. Note also that the performance of block SpMV generally improves with

increasing blocksize  $n_b$  since each matrix element has to be loaded only once from memory and can be reused for all block vector entries with the same row index. On the other hand, vector entries may have to be reread from main memory due to capacity misses. These effects can be accounted for by a slight modification of Eq. (4), which is relevant for the node-level performance analysis of SpMV [20] but not for the communication characteristics.

The number of vector entries fetched from remote processes during evaluation of Eq. (1) is

$$n_{vc} = |\{j : A_{ij} \neq 0 \text{ for } i \in [a:b], j \notin [a:b]\}|, \quad (5)$$

which results in the inter-process communication volume

$$V_c = n_b n_{vc} S_d. \quad (6)$$

$n_{vc}$  varies strongly with the sparsity pattern and cannot be replaced by an average value.

With memory traffic  $V_m$  and communication volume  $V_c$ , the execution time of SpMV is

$$t = \max_{\text{processes}} \left( \frac{V_m}{b_m} + \frac{V_c}{b_c} \right), \quad (7)$$

where  $b_m$  is the memory bandwidth and  $b_c$  is the (effective) inter-process communication bandwidth. Note that  $b_m, b_c$  are measured per process: If multiple processes share resources, for example the main memory interface on the same node, the bandwidth must be scaled accordingly.

For perfect overlap of local memory accesses and communication, the sum in Eq. (7) can be replaced by  $\max\{V_m/b_m, V_c/b_c\}$ . Perfect overlap is usually a too optimistic assumption, since also communication involves memory traffic due to MPI buffer access.

Note further that in Eq. (7) we assume that the communication volume is large enough to ignore network latency, but not so large to result in network congestion with significantly reduced throughput. These assumptions are in accordance with the benchmark results given below.

*Communication metrics.* To quantify the impact of communication on distributed SpMV we introduce three essentially equivalent metrics. The metrics are computed directly from the matrix sparsity pattern, prior to any benchmarks. In this way, they characterize the matrix rather than the execution time of a sparse matrix-vector operation which depends on additional factors such as the memory and communication bandwidth or the blocksize (see Eq. (7) for SpMV or Eq. (12) for the Chebyshev filter). Note that the metrics depend on how the matrix rows are distributed across the  $N_p$  processes. We here give the metrics for a uniform distribution, as specified after Eq. (1), such that they depend only on  $N_p$ . All metrics assume the value zero for  $N_p = 1$ .

The first metric is the ratio between remote and local memory accesses,

$$\chi_1 = \max_{\text{processes}} \frac{n_{vc}}{n_{vm}}. \quad (8)$$

It distinguishes memory-bound from communication-bound SpMVs: For  $\chi_1 \gg b_c/b_m$  the execution time of the SpMV according to Eq. (7) is dominated by communication, for  $\chi_1 \ll b_c/b_m$  by local memory access.

The second metric quantifies the communication volume of SpMV relative to the vector dimension  $D$ ,

$$\chi_2 = \sum_{\text{processes}} \frac{n_{vc}}{D}. \quad (9)$$

We can interpret this metric in the way that after approximately  $\chi_2^{-1}$  SpMVs the equivalent of a full vector has been communicated.

The third metric

$$\chi_3 = N_p \times \max_{\text{processes}} \frac{n_{vc}}{D} \quad (10)$$



Table 1. Communication metrics for the Exciton and Hubbard matrices.

matrix	$N_p$	$\chi_{1,3}$	$\chi_2$	matrix	$N_p$	$\chi_{1,3}$	$\chi_2$
Exciton, L=75	2	0.01	0.01	Hubbard, n_sites=14, n_fermions=7	2	0.54	0.54
	4	0.05	0.04		4	1.51	1.02
	8	0.11	0.09		8	2.52	1.53
	16	0.21	0.20		16	3.37	2.07
	32	0.42	0.41		32	4.17	2.65
$D = 10\,328\,853$	64	0.85	0.83	$D = 11\,778\,624$	64	5.58	3.19
$n_{\text{nzt}} = 8.96$				$n_{\text{nzt}} = 14.00$			
Exciton, L=200	2	0.00	0.00	Hubbard, n_sites=16, n_fermions=8	2	0.53	0.53
	4	0.02	0.01		4	1.50	1.01
	8	0.04	0.03		8	2.50	1.51
	16	0.08	0.07		16	3.37	2.03
	32	0.16	0.15		32	4.21	2.61
$D = 193\,443\,603$	64	0.32	0.31	$D = 165\,636\,900$	64	5.67	3.16
$n_{\text{nzt}} = 8.99$				$n_{\text{nzt}} = 16.00$			

quantifies how communication limits the parallel efficiency of SpMV. The parallel efficiency  $\Pi = t[1]/(N_p t[N_p])$  measures how the execution time  $t[N_p]$  scales with the number of processes  $N_p$ . For ideal scaling, where  $t[N_p] = t[1]/N_p$ , we have  $\Pi = 1$ , otherwise  $\Pi < 1$ .

In terms of the metric  $\chi_3$ , we can formulate the estimate

$$\Pi \lesssim \min\{1, \chi_3^{-1} \frac{b_c}{b_m}\} . \quad (11)$$

To see why, note that according to Eqs. (4), (7) the execution time on a single compute process is  $t[1] = V_m/b_m = (n_b S_d/b_m) \times D$  (if we neglect data traffic from matrix elements for large  $n_b$  and assume  $n_{\text{vm}} = D$ ). For distributed SpMV on  $N_p > 1$  processes we get the ideal speedup  $t[1]/t[N_p] = N_p$  if no communication is required (and if  $n_{\text{vm}}$  scales as  $D/N_p$ , which is a safe assumption). With communication the execution time is at least  $t[N_p] \geq V_c/b_c = (n_b S_d/b_c) \times n_{\text{vc}}$ , which results in the reduced parallel efficiency  $\Pi = t[1]/(N_p t[N_p]) \leq (b_c/b_m) \times D/(N_p n_{\text{vc}})$ . With the definition of  $\chi_3$  we arrive at the given bound on  $\Pi$ .

Under reasonable assumptions, the three metrics  $\chi_{1,2,3}$  are equivalent up to small factors. First, recall that we almost always have  $n_{\text{vm}} \approx D/N_p$  in Eq. (8), that is  $\chi_1 \approx \chi_3$ . Second, unless the communication volume per process varies strongly, it does not make a difference whether we take the maximum or average over all processes. Therefore, we also have  $\chi_2 = N_p \times (1/N_p) \sum_{\text{processes}} (n_{\text{vc}}/D) \approx N_p \max_{\text{processes}} (n_{\text{vc}}/D) = \chi_3$ , but a small factor may appear in this relation. A large discrepancy between  $\chi_{1,3}$  and  $\chi_2$ , say above a factor of 2...3, indicates a severe imbalance in the communication volume between the processes. Then, a careful implementation may try to adjust the distribution of rows onto processes to equalize the communication volume.

### 3.2 Communication metrics of real application matrices

Table 1 lists the communication metrics for the Exciton and Hubbard matrices from Fig. 1. The matrices are taken from the Scalable Matrix Collection ScaMaC and can be generated in various sizes controlled by the problem parameters [1]. In ScaMaC notation, the matrices in Fig. 1 are called “Exciton, L=200” and “Hubbard, n\_sites=16, n\_fermions=8.”

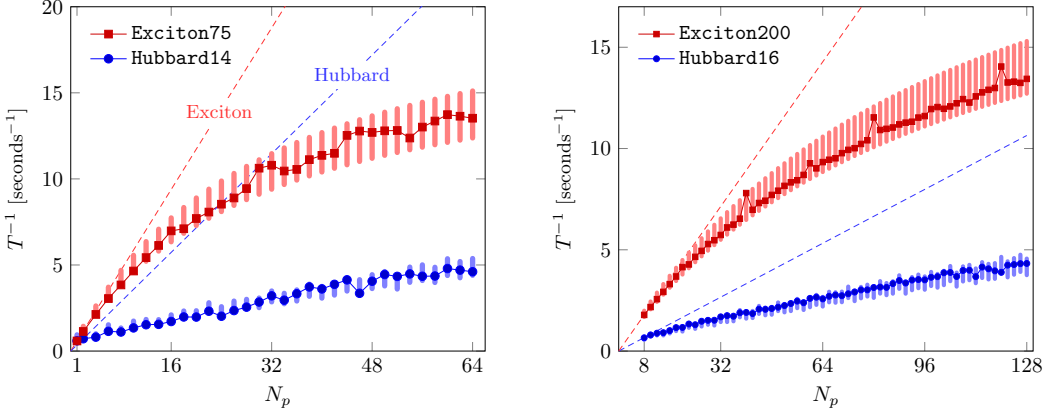


Fig. 4. Inverse execution time of one iteration of the Chebyshev filter (Alg. 2) as a function of the number of parallel processes. The vertical bars give the theoretical estimate according to Eq. (12), with a  $\pm 10\%$  variation of the model parameters  $b_c, \kappa$ . The dashed line corresponds to perfect strong scaling with parallel efficiency  $\Pi = 1$ ; in the right panel, the execution time for  $N_p = 8$  processes is used as a baseline. The left (right) panel uses  $n_b = 64$  ( $n_b = 8$ ) vectors.

The Exciton matrix is essentially a 3D stencil with additional local blocks. The communication metrics are small, which fits the “tame” sparsity pattern in Fig. 1. On the other hand, the “rugged” sparsity pattern of the Hubbard matrix results in large values of the communication metrics. From the values in Table 1 we see that  $\chi > 0.5$  already for  $N_p \geq 2$ . Using our previous estimates we expect that communication dominates SpMV in this situation.

**Benchmarks.** To test the predictive power of the communication metrics, Fig. 4 shows benchmark results for the Chebyshev filter in Algorithm 2, with the four matrices from Table 1. The benchmarks have been executed on the “Meggie” cluster at Erlangen National High Performance Computing Center (NHR@FAU)<sup>1</sup>. Clearly, the execution time of SpMV depends on the mapping of processes onto compute nodes. For all benchmarks, we use a NUMA-friendly “one process per socket” mapping [14]. On the Meggie cluster, this corresponds to two MPI processes per node, with 10 OpenMP threads each. Data in the left panel of Fig. 4 are obtained on  $1 \leq N_p \leq 32$  nodes, and include the data point  $N_p = 1$  for a single process on one socket (no communication). Data in the right panel are obtained on  $4 \leq N_p \leq 64$  nodes; at least  $N_p \geq 4$  nodes are required due to memory demands for the larger matrices.

We can now compare the benchmark results to the theoretical prediction of the model in Eq. (7) for the execution time of one iteration of the Chebyshev filter on  $N_p$  processes and  $n_b$  vectors,

$$T = \left[ \left( \frac{(S_d + S_i)n_{\text{nzr}}}{n_b} + \kappa S_d \right) \frac{1}{b_m} + \chi[N_p] \frac{S_d}{b_c} \right] \times n_b \times \frac{D}{N_p}. \quad (12)$$

This expression has three model parameters  $b_m, b_c, \kappa$ , while  $\chi[N_p]$  is not a parameter but computed from the matrix sparsity pattern as in Table 1. Generally, the blocksize  $n_b$  is large enough (we always have  $n_b \geq 8$ ) to allow us to neglect the first term for the memory traffic from the matrix at least in the qualitative estimates given later.

<sup>1</sup>Hardware documentation is available at

<https://hpc.fau.de/systems-services/systems-documentation-instructions/clusters/meggie-cluster/>

Table 2. Model parameters  $b_m, b_c, \kappa$  for the data in Fig. 4. Values marked with a \* are taken from the row(s) immediately above. Especially the value of  $b_m$  (from the STREAM benchmark) is the same for all matrices.

matrix	$b_m$ [GB s <sup>-1</sup> ]	$\kappa$	$b_c$ [GB s <sup>-1</sup> ]
Exciton75	53.3	7.30	2.82
Exciton200	*	*	3.10
Hubbard14	*	10.0	2.82
Hubbard16	*	*	2.54

To determine the model parameters we can measure the bare memory bandwidth  $b_m$  with the STREAM benchmark [26]. The parameter  $b_c$ , on the other hand, is an effective communication bandwidth that has to account for all communication-related operations in the SpMV, including the copying of halo elements to MPI buffers and other MPI overhead. On typical compute clusters we can expect a factor  $b_m/b_c^{\text{bare}} \approx 10 \dots 20$  between the memory bandwidth and the bare communication bandwidth  $b_c^{\text{bare}}$  of the cluster interconnect. Apart from highly idealized situations, the value of the effective  $b_c$  cannot be derived from  $b_c^{\text{bare}}$ . Instead, we use a single value of  $b_c$  for each curve in Fig. 4, which is obtained from a fit to the benchmark data. Including the communication-related overhead in SpMV a factor  $b_c^{\text{bare}}/b_c$  in the range  $1 \dots 2$  appears to be a reasonable fit result.

The factor  $\kappa$  in Eq. (12) accounts for reading and writing of the vectors  $W_1, W_2, V$  from and to memory in Algorithm 2. With ideal cache usage, we have  $\kappa = 5$  since  $W_1$  is read once from memory, and  $W_2, V$  are read and written. If instead of a fused kernel the two operations in step 7 are executed independently, the factor increases to  $\kappa = 6$  since  $W_2$  has to be read twice (for large problems it is likely that  $W_2$  has been evicted from cache after the SpMV). For an isolated SpMV, without the axpby operation, the factor would reduce to  $\kappa = 3$ .

In practice, cache usage is never ideal but vector entries have to be read more than once from memory due to capacity misses [20], resulting in  $\kappa > 5$ . The precise value depends on a number of conditions, especially how regular or scattered the memory access is. We determine the parameter  $\kappa$  from the benchmark for a single process ( $N_p = 1$ ) and use this value for all  $N_p \geq 1$ . Although this is an oversimplification since  $\kappa$  changes with the distribution of the matrix onto the processes, this choice agrees sufficiently well with the benchmark data.

The values of the model parameters for the four matrices in Fig. 4 are given in Table 2. The values are consistent with our basic assumptions. First, we have  $\kappa > 5$ , and  $\kappa$  is larger for the Hubbard matrix with the more irregular memory access. Second, the effective communication bandwidth  $b_c$  lies consistently within a  $\pm 10\%$  range across the four matrices, and the ratio  $b_m/b_c \approx 15 \dots 20$  is compatible with our expectations for the effective communication bandwidth of our SpMV.

Note that once  $b_m, b_c, \kappa$  are fixed in Eq. (12), the entire dependence of  $T$  on  $N_p$  arises from the communication metric  $\chi[N_p]$ , which is computed independently of the model parameters or benchmark data. As Fig. 4 shows, the theoretical prediction agrees very well with the benchmark data for all values of  $N_p$ , which validates our model.

Further evidence for our model is that all terms in Eq. (12) are required for agreement between model and benchmarks. Without the first term from local memory traffic the model would predict  $T = 0$  for  $N_p = 1$  since  $\chi[1] = 0$  (no communication for a single process). This is of course not correct. Without the explicit dependence of the communication metric  $\chi$  on  $N_p$  in the second term the model would predict perfect scaling  $T \propto 1/N_p$ . This is not correct as shown by the dashed lines in Fig. 4. In particular we cannot replace  $\chi[N_p]$  with a constant.

The behavior of the communication metrics in Table 1 and of the benchmark data in Fig. 4 is not specific to the Exciton or Hubbard matrices but of general nature. Appendix A lists communication metrics and benchmark results for various other matrices from ScaMaC. In all cases, our theoretical model agrees very well with the benchmark data. The appendix also shows that matrices with significant communication overhead in SpMV, reflected by large values of  $\chi$ , are not uncommon.

### 3.3 Panel layout speedup

So far, we have analyzed the execution time of the Chebyshev filter as a function of the number  $N_p$  of processes used for the parallel evaluation of the SpMV. In terms of vector layouts (see Fig. 3) the analysis applies to the standard stack layout where the sparse matrix rows, hence the vectors, are distributed equally across all the  $N_p$  processes.

We now turn to the concept of two orthogonal layers of parallelism. Our goal is to use Eq. (12) to estimate the speedup that can be achieved if the Chebyshev filter is evaluated in a panel layout instead of the stack layout. Recall that we can vary the shape of the panel layout provided that the total number  $\mathcal{P} = N_{\text{row}} \times N_{\text{col}}$  of processes remains fixed.

In a panel layout the SpMVs in the Chebyshev filter are executed simultaneously and independently in each of the process columns. Each SpMV uses a fraction  $N_p = \mathcal{P}/N_{\text{col}} = N_{\text{row}}$  of all processes and is applied to  $n_b = N_s/N_{\text{col}}$  vectors. The stack layout corresponds to  $N_{\text{col}} = 1$ , with  $N_p = \mathcal{P}$  and  $n_b = N_s$ . The two parameters in Eq. (12) that change between the stack and panel layout thus are  $N_p$  and  $n_b$ . With these parameters also the value of the communication metric  $\chi[N_p]$  changes. Note that the last factor  $n_b \times (D/N_p) = N_s D/\mathcal{P}$  in Eq. (12) is constant.

With the respective parameter values the execution time of the Chebyshev filter is

$$T_{\text{stack}} = T[\mathcal{P}, N_s] = S_d \times \left( \frac{\kappa}{b_m} + \frac{\chi[\mathcal{P}]}{b_c} \right) \times \frac{N_s D}{\mathcal{P}} \quad (13)$$

in the stack layout and

$$T_{\text{panel}} = T\left[\frac{\mathcal{P}}{N_{\text{col}}}, \frac{N_s}{N_{\text{col}}}\right] = S_d \times \left( \frac{\kappa}{b_m} + \frac{\chi[\mathcal{P}/N_{\text{col}}]}{b_c} \right) \times \frac{N_s D}{\mathcal{P}} \quad (14)$$

in the panel layout. For the sake of clarity, we omit in both expressions the memory traffic from the matrix elements (this is the first term in Eq. (12)), which is justified for reasonable values of  $n_b$ .

The speedup of the panel relative to the stack layout is

$$s = \frac{T_{\text{stack}}}{T_{\text{panel}}} = \frac{\kappa(b_c/b_m) + \chi[\mathcal{P}]}{\kappa(b_c/b_m) + \chi[\mathcal{P}/N_{\text{col}}]} \quad (15)$$

In the communication-bound regime  $\chi \gg \kappa(b_c/b_m)$ , the speedup is given by

$$s \simeq \frac{\chi[\mathcal{P}]}{\chi[\mathcal{P}/N_{\text{col}}]} \quad (16)$$

and depends entirely on the communication metric.

Figure 5 shows benchmark results for the speedup  $s$  for different shapes of the panel layout, in comparison to the theoretical prediction from Eq. (15). Again, we find very good agreement. Notably, even for the exciton matrices with the “tame” sparsity pattern and small values  $\chi < 1$  of the communication metric a significant speedup  $s > 2$  can be observed.

Note that the maximal speedup is achieved for  $N_{\text{col}} = \mathcal{P}$ , i.e., for the pillar layout, where SpMV does not require communication. If considered in isolation the pillar layout would result in perfect (weak and strong) scaling of the Chebyshev filter with parallel efficiency  $\Pi[\text{pillar}] = 1$ . However, in FD the Chebyshev filter is used in conjunction with orthogonalization, which cannot be performed in a scalable or efficient way in the pillar layout since entire vectors would have to be communicated.

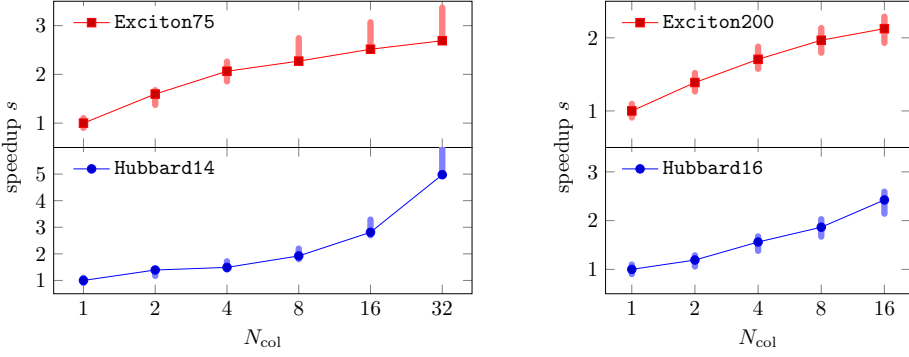


Fig. 5. Speedup of the Chebyshev filter in the panel layout relative to the stack layout, as a function of the number of process columns  $N_{\text{col}}$  ( $N_{\text{col}} = 1$  gives the stack layout, hence  $s = 1$ ). Data in the left (right) panel are obtained on 32 (64) nodes. For the larger matrices in the right panel a minimum of four nodes is required due to memory demands from storing the matrix, hence  $N_{\text{col}} \leq 16$ .

### 3.4 Redistribution of vectors between the panel and stack layout

Orthogonalization of vectors in the panel layout requires communication of vector entries along the horizontal axis of Fig. 3. Since every vector has to be matched against every other vector, the aggregated communication volume is at least of order  $N_s D (1 - 1/N_{\text{col}})$  vector entries. It is not obvious how to organize the “all-to-all” communication of vectors in the panel layout, especially since memory consumption becomes problematic if vectors are gathered at one (or at every) process.

Because of these difficulties we do not orthogonalize vectors in the panel layout but instead redistribute vectors between the panel and stack layout. Redistribution of vectors is a global operation with a controlled communication pattern. The communication volume is of the same order as for (the hypothetical) orthogonalization in the panel layout. Redistribution can be performed in-place, and does not require additional memory. Once vectors are in the stack layout, the known communication-avoiding orthogonalization techniques can be used.

Consider  $N_s$  vectors  $V_0, \dots, V_{N_s-1}$  with dimension  $D$  that are distributed across  $\mathcal{P}$  processes once in the stack, once in the panel layout (see Fig. 6). As before, the vectors are arranged as the columns of a  $D \times N_s$  matrix  $V$ , such that  $V_{ij}$  is the  $i$ -th entry of the  $j$ -th vector  $V_j$ .

The stack layout is specified by row indices  $k_0, \dots, k_{\mathcal{P}}$  that slice the range  $[0:D]$ , such that  $0 = k_0 \leq k_1 \leq \dots \leq k_{\mathcal{P}-1} \leq k_{\mathcal{P}} = D$ . Process  $i_{\text{row}}$ , with index  $i_{\text{row}} \in [0:\mathcal{P}]$ , stores a horizontal slice of the matrix  $V$ , given by the vector entries  $V_{ij}$  with  $i \in [k_{i_{\text{row}}}:k_{i_{\text{row}}+1}]$  and  $j \in [0:N_s]$ . These are  $N_s(k_{i_{\text{row}}+1} - k_{i_{\text{row}}})$  vector entries in total, that is about  $N_s D / \mathcal{P}$  for nearly equidistant row indices.

The  $N_{\text{row}} \times N_{\text{col}}$  panel layout is specified by row indices  $m_0, \dots, m_{N_{\text{row}}}$  that slice the range  $[0:D]$  and column indices  $n_0, \dots, n_{N_{\text{col}}}$  that slice the range  $[0:N_s]$ . Process  $(i_{\text{row}}, j_{\text{col}})$  stores a rectangular part of the matrix  $V$ , given by the vector entries  $V_{ij}$  with  $i \in [m_{i_{\text{row}}}:m_{i_{\text{row}}+1}]$  and  $j \in [n_{j_{\text{col}}}:n_{j_{\text{col}}+1}]$ . These are  $(m_{i_{\text{row}}+1} - m_{i_{\text{row}}})(n_{j_{\text{col}}+1} - n_{j_{\text{col}}})$  vector entries in total, that is about  $(D/N_{\text{row}})(N_s/N_{\text{col}}) = N_s D / \mathcal{P}$  for nearly equidistant row and column indices. This number agrees with the number of vector entries in the stack layout.

To redistribute vectors between the stack and panel layout we have to communicate vector entries horizontally in the graphical representation of Fig. 6. Redistribution of vectors from the stack to the panel layout and from the panel to the stack layout are inverse operations. The communication patterns are identical, only the direction of communication changes.

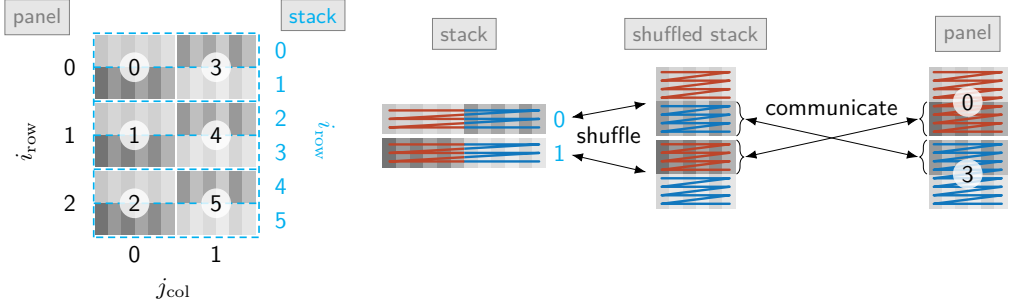


Fig. 6. Left:  $3 \times 2$  panel vs stack layout, with process ranks assigned in column-major order to the Cartesian grid of the panel. Right: Redistribution of vectors between the stack and panel layout requires shuffling of the stack (a local operation without communication) to preserve contiguous memory storage of vector entries (which are in row-major order, indicated by the zigzag lines) and horizontal communication of vector entries between processes. For the matching  $3 \times 2$  layout shown here, communication occurs only between the two processes in the same row of the panel.

Most communication takes place between processes in the same row of the panel layout. For matching layouts, where exactly  $m_{i_{\text{row}}} = k_{(i_{\text{row}} \times N_{\text{col}})}$ , communication strictly takes place between processes in the same row only. The general communication pattern for arbitrary choices of row and column indices involves technical details of minor relevance and is omitted here. In our implementation, communication is performed with a collective MPI\_Alltoall operation. Redistribution also requires shuffling of vector entries to preserve contiguous memory storage during and after the MPI operations. For row-major order as depicted in Fig. 6, we shuffle vector entries in the stack layout, for column-major order we would shuffle vector entries in the panel layout. Shuffling is a strictly local operation without communication.

Note that in Fig. 6 we assign process ranks in column-major order to the Cartesian grid of the panel layout. This choice puts “adjacent processes” with nearby rank into the same column of the panel, to acknowledge the fact that SpMV involves communication along the process columns. In any case, the process indices  $(i_{\text{row}}, j_{\text{col}})$  in the panel layout, or  $i_{\text{row}}$  in the stack layout, are logical indices rather than physical ranks and can be assigned freely. Which assignment is most efficient depends on the network topology.

To quantify the communication volume of redistribution we note that a process has to exchange all vector entries apart from those that lie in overlapping regions of the two layouts. In Fig. 6, the top left rectangle and the bottom right rectangle in each process row (colored in light gray in the figure) overlap and do not need to be communicated. The height (or width) of such a region is approximately  $D/\mathcal{P}$  (or  $N_s/N_{\text{col}}$ ). Therefore, the communication volume per process is approximately  $N_s D/\mathcal{P} - (D/\mathcal{P})(N_s/N_{\text{col}}) = (N_s D/\mathcal{P})(1 - 1/N_{\text{col}})$  vector entries. Summation over all columns gives the communication volume

$$\frac{V_{\text{row}}}{S_d} = N_s D \frac{N_{\text{col}} - 1}{\mathcal{P}} = N_s \frac{D}{N_{\text{row}}} (1 - 1/N_{\text{col}}) \quad (17)$$

per process row, and the total communication volume

$$\frac{V}{S_d} = N_s D (1 - 1/N_{\text{col}}) . \quad (18)$$

These values are exact for matching layouts, and reproduce our initial estimate.

### 3.5 Amortization of redistribution of vectors to the panel layout

For the Chebyshev filter, Fig. 4 shows how scaling is lost in the stack layout due to communication, while Fig. 5 shows how parallel efficiency can be regained in the panel layout. In FD, the Chebyshev filter does not occur in isolation but in conjunction with orthogonalization. Scaling and parallel efficiency of FD thus depend both on the speedup of the Chebyshev filter in the panel layout and the additional time for redistribution of vectors between the stack and panel layout.

To evaluate the Chebyshev filter in the panel layout and perform orthogonalization in the stack layout we have to redistribute vectors twice (steps 7, 9 in Alg. 1). Whether the cost of redistribution is amortized by the speedup of the Chebyshev filter depends on three numbers: (i) the speedup  $s = T_{\text{stack}}/T_{\text{panel}} > 1$  of a single iteration of the Chebyshev filter in the panel layout, (ii) the execution time  $T_{\text{rd}}$  of redistribution, which we can express in terms of Chebyshev filter iterations by the factor  $r = T_{\text{rd}}/T_{\text{panel}} > 1$  (that is, one redistribution corresponds to  $r$  SpMV's in the panel layout), (iii) the number of iterations in the Chebyshev filter, given by the degree  $n$  of the filter polynomial.

Combining the three numbers, the speedup of the Chebyshev filter in the panel layout relative to the stack layout, now including the time for redistribution, is

$$S = \frac{nT_{\text{stack}}}{nT_{\text{panel}} + 2T_{\text{rd}}} = s \frac{n}{n + 2r} . \quad (19)$$

Therefore, switching to the panel layout becomes favorable (i.e.,  $S > 1$ ) for

$$n > n^* = \frac{2r}{s - 1} . \quad (20)$$

The asymptotic speedup for  $n \gg n^*$  is  $S \approx s$ .

We can now make the connection to the communication metric  $\chi$  (with  $\chi \approx \chi_2 \approx \chi_{1,3}$ ). The speedup  $s$  is already given in Eq. (15). For the factor  $r$  we compare the communication volume of redistribution in Eqs. (17), (18) with the execution time according to Eq. (14) and find

$$r = \frac{1 - 1/N_{\text{col}}}{\kappa b_c/b_m + \chi[\mathcal{P}/N_{\text{col}}]} . \quad (21)$$

These values can be used in Eqs. (19), (20). In the communication-bound regime  $\chi \gg \kappa(b_c/b_m)$ , we have  $s \approx \chi[\mathcal{P}]/\chi[\mathcal{P}/N_{\text{col}}]$  as in Eq. (16) and  $r \approx (1 - 1/N_{\text{col}})/\chi[\mathcal{P}/N_{\text{col}}]$  (recall our interpretation of  $\chi$  that the equivalent of a full vector is communicated every  $\chi^{-1}$  SpMV's). Our analysis thus predicts, up to small factors, that it is favorable to switch to a panel layout with  $N_{\text{col}} > 1$  if

$$n > \frac{2(1 - 1/N_{\text{col}})}{\chi[\mathcal{P}] - \chi[\mathcal{P}/N_{\text{col}}]} . \quad (22)$$

For larger values of  $\chi[\mathcal{P}]$  the condition is fulfilled already for smaller values of  $n$ .

For the pillar layout, with  $N_{\text{col}} = \mathcal{P}$ , the condition simplifies to

$$n_{[\text{pillar}]} \geq \frac{2}{\chi[\mathcal{P}]} , \quad (23)$$

since  $\chi[1] = 0$  and  $(1 - 1/N_{\text{col}}) < 1$ . This condition is fulfilled for *any*  $n \geq 1$  if  $\chi[\mathcal{P}] \geq 2$ . For the Hubbard matrices this is the case already for  $\mathcal{P} \geq 16$  (see Table 1). In this situation it is *always* favorable to switch to a pillar layout for evaluation of the Chebyshev filter, even for  $n = 1$ .

Numerical values for our example matrices are collected in Table 3. The two empirical values in the table measured in the benchmarks are the speedup of the Chebyshev filter, identical to Fig. 5, and the factor  $r$  quantifying redistribution of vectors. From these two values we compute the break even point  $n^*$  according to Eq. (20) and the speedup  $S$  for  $n > n^*$  according to Eq. (19). Since we now include the time for redistribution of vectors, the speedup  $S$  is smaller than the speedup  $s$

Table 3. Amortization of redistribution of vectors. The numbers are for  $\mathcal{P} = 32$  ( $\mathcal{P} = 64$ ) processes for the Exciton75 and Hubbard14 (Exciton200 and Hubbard16) matrices. For the larger matrices, the available memory required to store the sparse matrix restricts the data to  $N_{\text{row}} \geq 4$ , that is  $N_{\text{col}} \leq 16$ . The additional data for  $N_{\text{col}} = 64^*$  are obtained with the matrix-free SpMV used for the FD computations in Sec. 4, which has slightly lower node-level performance.

matrix	$N_{\text{col}}$	$s$	$r$	$n^*$	speedup $S$ for $n$ spMV				
					$n = 10$	$n = 20$	$n = 30$	$n = 50$	$n = 100$
Exciton75	2	1.60	4	14	—	1.14	1.26	1.38	1.48
—	8	2.27	8	13	—	1.26	1.48	1.72	1.96
—	32 [pillar]	2.69	9	11	—	1.42	1.68	1.98	2.28
Hubbard14	2	1.39	1	6	1.16	1.26	1.30	1.34	1.36
—	8	1.92	2	5	1.37	1.60	1.69	1.78	1.85
—	32 [pillar]	4.98	4	2	2.77	3.56	3.93	4.29	4.61
Exciton200	2	1.39	17	87	—	—	—	—	1.04
—	8	1.97	27	56	—	—	—	—	1.28
—	16	2.13	31	54	—	—	—	—	1.31
—	64* [pillar*]	2.02	29	56	—	—	—	—	1.28
Hubbard16	2	1.19	2	21	—	—	1.05	1.10	1.14
—	8	1.86	4	9	1.03	1.33	1.47	1.60	1.72
—	16	2.42	5	7	1.21	1.61	1.81	2.02	2.20
—	64* [pillar*]	7.25	15	5	1.81	2.90	3.62	4.53	5.58

of the isolated Chebyshev filter. For a large number of SpMV's ( $n \gg n^*$ ), the speedup reaches its maximal value ( $S \rightarrow s$ ). Especially in the pillar layout  $N_{\text{col}} = \mathcal{P}$  this coincides with the parallel efficiency reaching the optimum value  $\Pi \rightarrow 1$ .

Recall that for the isolated Chebyshev filter the pillar layout offers perfect weak scaling: The execution time for  $\mathcal{P} \times N_s$  vectors on  $\mathcal{P}$  nodes is identical to the execution time for  $N_s$  vectors on a single node. As a consequence, the pillar layout is always the most favorable vector layout for large  $n$ , when the cost of redistribution is amortized by the speedup of the Chebyshev filter.

#### 4 FILTER DIAGONALIZATION WITH TWO LAYERS OF PARALLELISM

The Exciton and Hubbard matrices in Table 1 are not merely artificial test cases for our communication metrics but appear in quantum physics research problems that require extraction of a large number of extremal or interior eigenvalues from tiny regions of the entire spectrum. In this respect, both problems pose a challenge for any eigensolver. As typical examples of the matrices found in quantum physics applications, the Exciton and Hubbard matrices have wildly different sparsity patterns and spectral properties but share a large matrix dimension.

The Exciton matrix appears in the modeling of an exciton, that is a bound electron-hole pair akin to a hydrogen atom in a semiconductor, in the cuprous oxide  $\text{Cu}_2\text{O}$ . In this material, even-parity exciton states exhibit strong deviations from the hydrogen-like Rydberg series “ $E_n = -E_0/n^2$ ” that can be traced back to spin-orbit coupling and crystal lattice effects on the kinetic energy of the electron and hole [17, 18]. To compute the exciton states we thus cannot reuse the textbook solution of the hydrogen atom but have to solve the full lattice problem [2, 3], which leads to the Exciton matrices. The matrix parameter  $L$  controls the truncation of the infinite quantum mechanical state



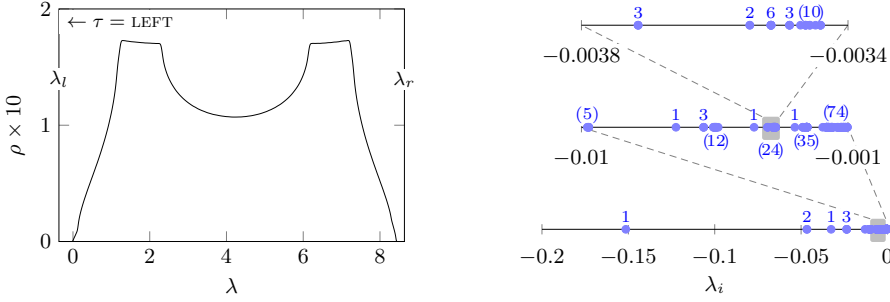


Fig. 7. Left panel: Density of states  $\rho(\lambda)$  of the Exciton200 matrix ( $D = 193\,443\,603$ ). Right panel: Eigenvalues near the left end of the spectrum, for  $\lambda_i < 0$ , at three levels of magnification. Blue numbers indicate the multiplicity of eigenvalues or, if in round brackets, the size of a cluster of nearly degenerate eigenvalues. The width of the interval  $[-0.0038, 0.0034]$  on top is smaller than  $5 \times 10^{-5}$  of the width of the entire spectrum; it still contains 24 eigenvalues (counted with multiplicities).

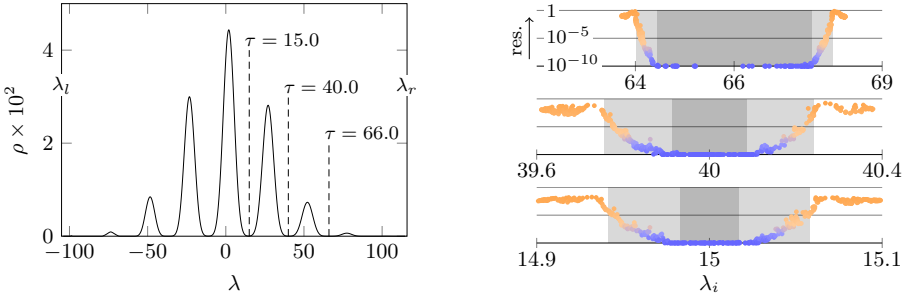


Fig. 8. Left panel: Density of states  $\rho(\lambda)$  of the Hubbard16 matrix ( $D = 165\,636\,900$ ). Additional matrix parameters in ScaMaC notation are  $U=25$ ,  $\text{ranpot}=1$  to create partially filled gaps with small density of states. Right panel: Eigenvalues near the targets  $\tau = 15.0, 40.0, 66.0$  inside of the spectrum. Distance to the horizontal axis indicates the residual of the eigenvectors, as shown in the top panel. Converged eigenvalues, with residual below  $10^{-10}$ , are found on the horizontal axis. The larger (smaller) gray rectangle indicates the search (target) interval.

space to a finite lattice. The matrix dimension is  $D = 3(2L + 1)^3$ . Computation of high excitonic states requires large values of  $L$ , here  $L = 200$ .

The left panel in Fig. 7 shows the density of states (DOS)  $\rho(\lambda)$  of the Exciton matrix, computed with the kernel polynomial method (KPM) [43]. The DOS gives the number of eigenvalues in an interval as  $|\{\lambda_i \text{ with } a \leq \lambda_i \leq b\}| = D \int_a^b \rho(\lambda) d\lambda$ . The matrix dimension  $D$  appears because we normalize the DOS to  $\int_{-\infty}^{\infty} \rho(\lambda) d\lambda = 1$ . The exciton states of interest appear at the left (lower) end of the spectrum, for  $\lambda_i < 0$ , below the much wider spectrum of unbound electron-hole pairs that cannot be excluded from the lattice problem. The values of  $\lambda_i$  correspond to the physical exciton energies measured in electron volt.

The right panel in Fig. 7 shows the exciton states with eigenvalues  $\lambda_i < 0$  as computed with FD. The exciton states are characterized by multiple clusters of (nearly) degenerate eigenvalues, which move closer together as  $\lambda_i$  approaches zero from below. This is reminiscent of the Rydberg series of the hydrogen atom. Resolution of eigenvalues within the clusters is required for comparison

Table 4. Summary of FD with the Exciton (Hubbard) matrix from Figs. 7, 8, with  $N_s = 384$  ( $N_s = 512$ ) search vectors on  $\mathcal{P} = 64$  compute nodes, and  $N_t = 100$  requested target vectors.

matrix	target	no. of SpMV's	relative target int.	width of search int.	conv. vecs.	runtime	no. of /time redistribution
Exciton200	LEFT	16 979	$4.0 \times 10^{-2}$	$4.1 \times 10^{-2}$	138	08:20:53	42/3.9%
[with $N_t = 50$ :		9 939	$4.0 \times 10^{-2}$	$4.1 \times 10^{-2}$	58	04:53:17	42/6.4%]
Hubbard16	$\tau = 15.0$	46 347	$1.5 \times 10^{-4}$	$5.3 \times 10^{-4}$	143	26:17:20	46/0.6%
—	$\tau = 40.0$	12 984	$7.8 \times 10^{-4}$	$2.2 \times 10^{-3}$	123	07:21:21	44/2.1%
—	$\tau = 66.0$	4 090	$1.4 \times 10^{-2}$	$1.8 \times 10^{-2}$	101	02:18:52	44/7.2%

with optical measurements of the exciton emission spectra, which achieve high accuracy and thus require equal accuracy of the numerical computation [17]. Using many search vectors, FD is oblivious to the clustered structure of the spectrum and can fully resolve all eigenvalues.

The Hubbard matrix appears in many-body quantum physics, where the Hubbard model is a paradigmatic model of strongly correlated electrons where Coulomb interaction leads to metal-insulator transitions or superconductivity [4, 9]. Recent research on, e.g., ultrafast control of quantum materials or many-body thermalization addresses physics associated with interior eigenvalues of the Hubbard (or related) matrices [10, 36, 37]. It is characteristic of many-body quantum physics that the dimension  $D = \binom{n_{\text{sites}}}{n_{\text{fermions}}}^2$  of the Hubbard matrix grows quickly with the physical problem size, given by the matrix parameters  $n_{\text{sites}}$ ,  $n_{\text{fermions}}$ .

The left panel in Fig. 8 shows the DOS of the Hubbard matrix computed with KPM, the right panel shows the eigenvalues computed with FD. To let the FD computations finish in reasonable time we chose (perhaps unphysical) matrix parameters ( $U=25$ ,  $\text{ranpot}=1$  in ScaMaC notation; both measured in units of the hopping matrix element  $t$ ), where partially filled gaps with small DOS appear in the spectrum. Note that in physics terms we deal with the many-body DOS of the Hubbard model; for the Hubbard16 matrix with 8 electrons per spin orientation the many-body DOS for large  $U$  has a peak in the center of the spectrum near  $\lambda = 0$  that corresponds to states with  $8/2 = 4$  doubly occupied sites. Computationally, in regions of large DOS the widths of the target and search interval become so tiny that the degree of the filter polynomial gets too large for our present demonstrations. The plain FD algorithm 1 has no strategy to remedy this situation; algorithmic improvements beyond the scope of the present work would become necessary. Therefore, we here use FD for targets  $\tau$  in the partially filled gaps.

Table 4 documents the performance of FD for the computations in Figs. 7, 8. The experiments were conducted in the following way: First, we implemented a matrix-free SpMV for the Exciton and Hubbard matrices. Then, since memory is required only for storage of vectors, we can use the pillar layout with  $N_s/\mathcal{P} = 6$  (8) search vectors per compute node for the Exciton (Hubbard) matrix<sup>2</sup>. In the pillar layout, the matrix-free implementation takes 1.77 s per SpMV for the Exciton200 matrix and 2.04 s per SpMV for the Hubbard16 matrix. These execution times are consistent with values extrapolated for  $N_p \rightarrow 1$  from the data in Fig. 4 (right panel), where we had to use  $N_p \geq 4$  compute nodes due to memory demands arising from explicit storage of the sparse matrix. We did not

<sup>2</sup>On the Meggie cluster, each node has 64 GiB main memory. The Exciton matrix has complex-valued entries (i.e.,  $S_d = 16$ ) while the Hubbard matrix is real (i.e.,  $S_d = 8$ ). Three copies of each search vector are required in the Chebyshev iteration in Alg. 2, resulting in 51.9 GiB (29.6 GiB) memory consumption per node for the Exciton200 (Hubbard16) matrix with 6 (8) search vectors per node.

invest further effort into optimization of the matrix-free SpMV routines because the unoptimized implementation will suffice to demonstrate the importance of (avoiding) communication.

The data in Table 4 supports the two key assumptions of the present work: First, the degree of the filter polynomial is large since the width of the target and search interval is small. FD requires about 20 iterations for convergence, with about  $2 \times 20 = 40$  redistributions of vectors (see last column). In the course of the iterations, the target and search intervals shrink to their final sizes, and the degree of the filter polynomial increases. For the Exciton200 matrix, the degree increases from  $n = 20$  in the first iteration to  $n = 1588$  in the final (twenty-first) iteration. Second, as a consequence of the large degree of the filter polynomial, the total number of SpMV is high and the cost of redistribution negligible (last column). For the Hubbard16 matrix, the last column shows how the percentage of the runtime spent on redistribution decreases even below 1% as the degree of the filter polynomial increases for targets  $\tau$  closer towards the center of the spectrum.

Table 4 also supports our two key messages for the practical application. First, filter diagonalization works: Despite the complicated structure of the spectrum (for the Exciton matrix) or the tiny size of the target interval (for the Hubbard matrix), FD successfully and reliably computes many eigenvectors and eigenvalues. While we cannot claim that the plain FD scheme of Alg. 1 is particularly sophisticated, advanced, or guarantees fast convergence, it seems that a massive block algorithm such as FD may have its own merits even in large-scale eigenvalues computations. Second, communication does not prevent scalability or parallel efficiency of large-scale eigenvalue computations if, but only if, one exploits the two layers of parallelism inherent to such computations. This is probably the central message of the present work.

To see that this message is indeed true, note that the negligible cost of redistribution documented in Table 4 implies that the scalability of FD depends only on the scalability of the Chebyshev filter. The Chebyshev filter in the pillar layout shows perfect weak scaling, and for sufficiently many vectors per process column even strong scaling. We can thus conclude that the entire FD computation scales (almost perfectly).

In fact, we now have enough benchmark data to quantify the speedup of FD in the pillar layout, even though we did not actually perform the computations in the stack layout needed for comparison because they would take too long. We can reason as follows: The execution time of the matrix-free SpMV in the pillar layout has been given above. The execution time of SpMV in the stack layout on  $\mathcal{P} = 64$  compute nodes can be taken from Fig. 4. In comparison we find that the speedup  $s$  of the Chebyshev filter in the pillar layout is  $s = 2.02$  ( $s = 7.25$ ) for the Exciton200 (Hubbard16) matrix (these values have been included in Table 3). The number of SpMVs in the present FD computations is two to four orders of magnitude larger than the break-even point  $n^*$ , such that we achieve the asymptotic speedup  $S \simeq s$ . In short, for the Exciton200 (Hubbard16) matrix the FD computation with two layers of parallelism is twice as fast (seven times faster) than a standard computation that uses only the one layer of parallelism offered by the stack layout.

Note that the speedup is already achieved with a default SpMV implementation. Careful optimization of the matrix-free SpMV routines might boost the node-level performance [27], and thus increase the speedup  $S$ . Higher node-level performance with faster local operations makes it even more important to avoid communication, which further strengthens our message.

## 5 SUMMARY & OUTLOOK

The main obstacle to scalability of large-scale distributed computations is communication. Preserving scalability and parallel efficiency thus requires strategies to minimize communication. In the present paper we introduce such a strategy for large-scale eigenvalue computations, using filter diagonalization (FD) as an example of an eigensolver with many search vectors. In such

eigensolvers we can identify two orthogonal layers of parallelism, which describe how vectors and sparse matrices are distributed in a general panel layout.

To minimize communication we must compare the different distributed vector layouts for the central operation of the eigensolver, sparse matrix-vector multiplication (SpMV). Communication is maximal in the standard stack layout, but can completely be avoided in the opposite extreme of the pillar layout. However, it is not obvious that the stack layout should be replaced by the pillar layout since SpMV and the second major operation in the eigensolver, which is orthogonalization, have competing communication patterns. Therefore, the question arises whether the cost of redistribution of vectors between different layouts is amortized by the speedup of SpMV.

To answer this question we introduce a metric  $\chi$  to quantify the communication volume of SpMV, which is directly derived from the matrix sparsity pattern. Benchmarks show that our model for the communication overhead of SpMV, based on the metric  $\chi$ , can accurately predict the speedup of SpMV in the different vector layouts. We can thus identify the conditions under which it is favorable to give up the standard stack layout in favor of a panel (or pillar) layout. Quite generally, these conditions are fulfilled for matrices with a “rugged” sparsity pattern and large values of  $\chi$ . But even for matrices with a “tame” sparsity pattern and small values of  $\chi$ , a speedup is achieved if a large number of SpMVs is executed.

The general scenario developed here is clearly observed in the exemplary FD computations for the large-scale Exciton and Hubbard matrices. Even for a stencil-like Exciton matrix, with values  $\chi < 1$ , the communication overhead of SpMV in the stack layout is large enough to achieve a speedup of 2 by switching to the pillar layout. For matrices of Hubbard-type, with  $\chi > 1$ , we can achieve almost an order of magnitude speedup. Note that for very large matrix dimension it will be impossible to use the pillar layout because of memory requirements, even with a matrix-free SpMV. In essence, the pillar layout trades memory for performance; if the memory requirements cannot be fulfilled, a less favorable panel layout must be chosen.

For the present paper we choose FD as our algorithmic example of an eigensolver with two layers of parallelism. Since the algorithmic performance of FD is not as good as one might expect from a general-purpose eigensolver, it is important to ask whether the current results on computational performance, in terms of preserving or restoring scalability and parallel efficiency, generalize to other algorithms. The two assumptions underlying our results are (i) we deal with a block eigensolver with multiple or many search vectors, and (ii) multiple SpMVs are executed in a row (more than the break-even point  $n^*$  derived in Eq. (20)). Under these assumptions, our results generalize to different eigensolvers or similar algorithms for other sparse linear algebra problems. One class of algorithms that might improve on the algorithmic shortcomings of FD are hybrid algorithms that combine Chebyshev filters and a few Arnoldi steps to construct a Krylov subspace. Whether such algorithms can be successfully applied to relevant large-scale eigenvalue problems, for example to the Hubbard model in regions with large DOS, remains to be demonstrated.

## 6 CODE AVAILABILITY

All data in the present work is generated with the FD code at <https://www.bitbucket.org/alvbit/twolayerfd>. The code is built on top of the GHOST library (<https://www.bitbucket.org/essex/ghost>) for distributed sparse-matrix and vector operations [21], and uses ScaMaC (<https://www.bitbucket.org/essex/matrixcollection>) for the generation of the different sparse matrices. The repository contains the `scamac_count_commvol` tool to compute the communication metrics directly from the sparsity pattern.

Table 5. Communication metrics for various ScaMaC matrices.

matrix	$N_p$	$\chi_{1,3}$	$\chi_2$	matrix	$N_p$	$\chi_{1,3}$	$\chi_2$
SpinChainXXZ, n_sites=24,n_up=12	2	0.52	0.52	TopIns,Lx=100, Ly=100,Lz=100	2	0.02	0.02
	4	1.50	1.01		4	0.08	0.06
	8	2.51	1.52		8	0.16	0.14
	16	3.40	2.00	$D = 4\,000\,000$ $n_{\text{nzr}} = 11.88$	16	0.32	0.30
	32	4.18	2.49		32	0.64	0.62
	64	5.15	3.05		64	1.28	1.26
SpinChainXXZ, n_sites=30,n_up=15	2	0.52	0.52	TopIns,Lx=500, Ly=500,Lz=500	2	0.00	0.00
	4	1.50	1.01		4	0.02	0.01
	8	2.49	1.51		8	0.03	0.03
	16	3.43	1.99	$D = 500\,000\,000$ $n_{\text{nzr}} = 11.98$	16	0.06	0.06
	32	4.27	2.47		32	0.13	0.12
	64	5.10	3.03		64	0.26	0.25

Table 6. Model parameters  $b_m, b_c, \kappa$  for the data in Fig. 9, with the same description as in Table 2.

matrix	$b_m$ [GB s <sup>-1</sup> ]	$\kappa$	$b_c$ [GB s <sup>-1</sup> ]
TopIns100	53.3	8.28	3.10
TopIns500	*	*	2.82
SpinChain24	*	12.2	3.52
SpinChain30	*	*	2.68

## ACKNOWLEDGMENTS

The authors would like to thank Dominik Ernst for help with the GHOST library. This project was funded by the *Competence Network for Scientific High Performance Computing in Bavaria* (KONWIHR). The authors gratefully acknowledge the scientific support and HPC resources provided by the Erlangen National High Performance Computing Center (NHR@FAU) of the Friedrich-Alexander-Universität Erlangen-Nürnberg (FAU). The hardware is funded by the German Research Foundation (DFG).

## A ADDITIONAL BENCHMARK DATA

Table 5 shows the communication metric  $\chi$  for the ScaMaC matrices SpinChainXXZ (which we used in Ref. [32]) and TopIns (which we used in Ref. [28]). The corresponding benchmarks are given in Fig. 9. Again, the model of Eq. (12) agrees very well with the benchmark data. The model parameters in Table 6 assume reasonable and consistent values across the different matrices. Instead of collecting further benchmark data or tables for the communication metric  $\chi$  we like to emphasize that both can be generated easily with the tools in the FD and ScaMaC repositories.

## REFERENCES

- [1] Andreas Alvermann. 2022. ScaMaC – A Scalable Matrix Collection. [www.bitbucket.org/essex/matrixcollection](http://www.bitbucket.org/essex/matrixcollection)
- [2] Andreas Alvermann and Holger Fehske. 2018. Exciton mass and exciton spectrum in the cuprous oxide. *J. Phys. B* 51, 4 (2018), 044001. <https://doi.org/10.1088/1361-6455/aaa060>

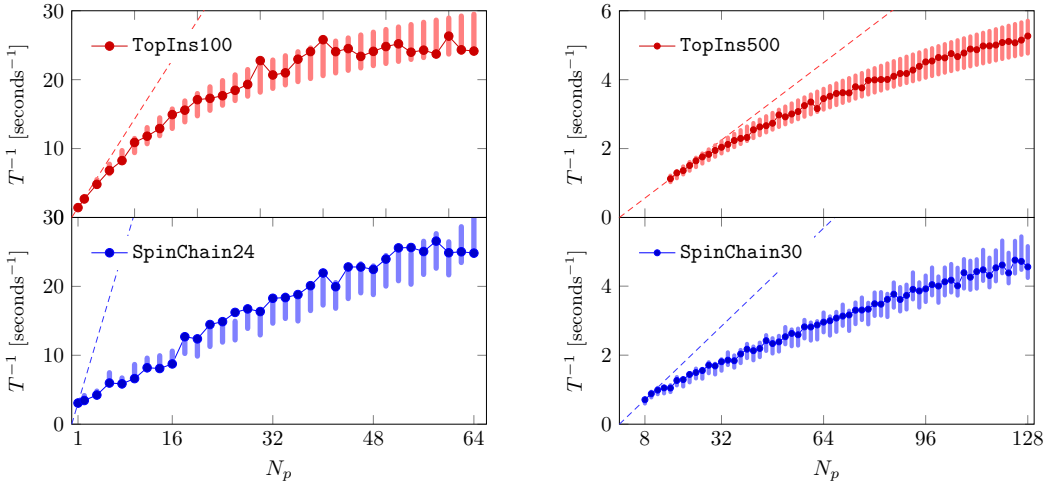


Fig. 9. Same plot as in Fig. 4, now for the SpinChainXXZ and TopIns matrices from Tab. 5. In the right panel, the execution time for  $N_p = 8$  (SpinChain30) or  $N_p = 16$  (TopIns500) processes is used as a baseline. The left (right) panel uses  $n_b = 64$  ( $n_b = 8$ ) vectors.

- [3] A. Alvermann, P. B. Littlewood, and H. Fehske. 2011. Variational discrete variable representation for excitons on a lattice. *Phys. Rev. B* 84 (Jul 2011), 035126. Issue 3.
- [4] Adolfo Avella and Ferdinando Mancini (Eds.). 2012. *Strongly Correlated Systems*. Springer, Berlin, Heidelberg. <https://doi.org/10.1007/978-3-642-21831-6>
- [5] R. Barrett, M. Berry, T. F. Chan, J. Demmel, J. Donato, J. Dongarra, V. Eijkhout, R. Pozo, C. Romine, and H. Van der Vorst. 1993. *Templates for the Solution of Linear Systems: Building Blocks for Iterative Methods*. SIAM, Philadelphia, PA.
- [6] L. S. Blackford, J. Choi, A. Cleary, E. D’Azevedo, J. Demmel, I. Dhillon, S. Hammarling, G. Henry, A. Petitet, K. Stanley, D. Walker, R. C. Whaley, and Jack J. Dongarra. 1997. *ScaLAPACK User’s Guide*. Society for Industrial and Applied Mathematics, USA. <https://netlib.org/scalapack/>
- [7] M. Bollhöfer, Y. Saad, and O. Schenk. 2016. ILUPACK—Preconditioning Software Package. [www.icm.tu-bs.de/~bolle/ilupack/](http://www.icm.tu-bs.de/~bolle/ilupack/).
- [8] Jane K. Cullum and Ralph A. Willoughby. 1985. *Lanczos Algorithms for Large Symmetric Eigenvalue Computations*. Vol. I & II. Birkhäuser, Boston.
- [9] E. Dagotto. 1994. Correlated electrons in high-temperature superconductors. *Rev. Mod. Phys.* 66 (1994), 763.
- [10] Alberto de la Torre, Dante M. Kennes, Martin Claassen, Simon Gerber, James W. McIver, and Michael A. Sentef. 2021. Colloquium: Nonthermal pathways to ultrafast control in quantum materials. *Rev. Mod. Phys.* 93 (Oct 2021), 041002. Issue 4. <https://doi.org/10.1103/RevModPhys.93.041002>
- [11] James Demmel, Laura Grigori, Mark Hoemmen, and Julien Langou. 2012. Communication-optimal Parallel and Sequential QR and LU Factorizations. *SIAM J. Sci. Comp.* 34 (Feb. 2012), 206–239.
- [12] Diederik R. Fokkema, Gerard L. G. Sleijpen, and Henk A. van der Vorst. 1998. Jacobi-Davidson style QR and QZ algorithms for the reduction of matrix pencils. *SIAM J. Sci. Comp.* 20 (1998), 94–125.
- [13] Martin Galgon, Lukas Krämer, Bruno Lang, Andreas Alvermann, Holger Fehske, Andreas Pieper, Georg Hager, Moritz Kreutzer, Faisal Shahzad, Gerhard Wellein, Achim Basermann, Melven Röhrig-Zöllner, and Jonas Thies. 2017. Improved Coefficients for Polynomial Filtering in ESSEX. In *Eigenvalue Problems: Algorithms, Software and Applications in Petascale Computing*, Tetsuya Sakurai, Shao-Liang Zhang, Toshiyuki Imamura, Yusaku Yamamoto, Yoshinobu Kuramashi, and Takeo Hoshi (Eds.). Springer International Publishing, Cham, 63–79.
- [14] Georg Hager and Gerhard Wellein. 2010. *Introduction to High Performance Computing for Scientists and Engineers*. CRC Press, Boca Raton.
- [15] Vicente Hernandez, Jose E. Roman, and Vicente Vidal. 2005. SLEPc: A scalable and flexible toolkit for the solution of eigenvalue problems. *ACM Trans. Math. Software* 31, 3 (2005), 351–362.
- [16] Sarah Huber, Yasunori Futamura, Martin Galgon, Akira Imakura, Bruno Lang, and Tetsuya Sakurai. [n.d.]. Flexible subspace iteration with moments for an effective contour integration-based eigensolver. *Numerical Linear Algebra*

- with Applications ([n.d.]), e2447. <https://doi.org/10.1002/nla.2447> (in press).
- [17] T. Kazimierzczuk, D. Fröhlich, S. Scheel, H. Stolz, and M. Bayer. 2014. Giant Rydberg excitons in the copper oxide  $\text{Cu}_2\text{O}$ . *Nature* 514 (2014), 343–347.
  - [18] Claus Klingshirn. 2007. *Semiconductor Optics* (third ed.). Springer, Berlin.
  - [19] Moritz Kreutzer, Dominik Ernst, Alan R. Bishop, Holger Fehske, Georg Hager, Kengo Nakajima, and Gerhard Wellein. 2018. Chebyshev Filter Diagonalization on Modern Manycore Processors and GPGPUs. In *High Performance Computing*, Rio Yokota, Michèle Weiland, David Keyes, and Carsten Trinitis (Eds.). Springer International Publishing, Cham, 329–349.
  - [20] Moritz Kreutzer, Georg Hager, Gerhard Wellein, Holger Fehske, and Alan R. Bishop. 2014. A Unified Sparse Matrix Data Format for Efficient General Sparse Matrix-Vector Multiplication on Modern Processors with Wide SIMD Units. *SIAM Journal on Scientific Computing* 36, 5 (2014), C401–C423. <https://doi.org/10.1137/130930352>
  - [21] Moritz Kreutzer, Jonas Thies, Melven Röhrig-Zöllner, Andreas Pieper, Faisal Shahzad, Martin Galgon, Achim Basermann, Holger Fehske, Georg Hager, and Gerhard Wellein. 2017. GHOST: Building Blocks for High Performance Sparse Linear Algebra on Heterogeneous Systems. *International Journal of Parallel Programming* 45, 5 (1 Oct 2017), 1046–1072. <https://doi.org/10.1007/s10766-016-0464-z>
  - [22] N. J. Lehmann. 1963. Optimale Eigenwerteinschlüssen. *Numer. Math.* 5 (1963), 246–272.
  - [23] R. B. Lehoucq, D. C. Sorensen, and C. Yang. [n.d.]. ARPACK Users’ Guide. <http://www.caam.rice.edu/software/ARPACK/>.
  - [24] R. Li, Y. Xi, L. Erlandson, and Y. Saad. 2019. The Eigenvalues Slicing Library (EVSL): Algorithms, Implementation, and Software. *SIAM Journal on Scientific Computing* 41, 4 (2019), C393–C415. <https://doi.org/10.1137/18M1170935> arXiv:<https://doi.org/10.1137/18M1170935>
  - [25] David J. Luitz. 2021. Polynomial filter diagonalization of large Floquet unitary operators. *SciPost Phys.* 11 (2021), 021. <https://doi.org/10.21468/SciPostPhys.11.2.021>
  - [26] John D. McCauley. 1995. Memory Bandwidth and Machine Balance in Current High Performance Computers. *IEEE Computer Society Technical Committee on Computer Architecture (TCCA) Newsletter* (Dec. 1995), 19–25.
  - [27] Andreas Pieper, Georg Hager, and Holger Fehske. 2021. A domain-specific language and matrix-free stencil code for investigating electronic properties of Dirac and topological materials. *The International Journal of High Performance Computing Applications* 35, 1 (2021), 60–77. <https://doi.org/10.1177/1094342020959423> arXiv:<https://doi.org/10.1177/1094342020959423>
  - [28] Andreas Pieper, Moritz Kreutzer, Andreas Alvermann, Martin Galgon, Holger Fehske, Georg Hager, Bruno Lang, and Gerhard Wellein. 2016. High-Performance Implementation of Chebyshev Filter Diagonalization for Interior Eigenvalue Computations. *J. Comp. Phys.* 325 (2016), 226–243. <http://dx.doi.org/10.1016/j.jcp.2016.08.027>
  - [29] Francesca Pietracaprina, Nicolas Macé, David J. Luitz, and Fabien Alet. 2018. Shift-invert diagonalization of large many-body localizing spin chains. *SciPost Phys.* 5 (2018), 45. Issue 5. <https://doi.org/10.21468/SciPostPhys.5.5.045>
  - [30] E. Polizzi. 2009. Density-matrix-based algorithm for solving eigenvalue problems. *Phys. Rev. B* 79 (2009), 115112.
  - [31] PARDISO Solver Project. 2022. <http://www.pardiso-project.org/>. Accessed: 2022-08-04.
  - [32] Melven Röhrig-Zöllner, Jonas Thies, Moritz Kreutzer, Andreas Alvermann, Andreas Pieper, Achim Basermann, Georg Hager, Gerhard Wellein, and Holger Fehske. 2015. Increasing the performance of the Jacobi-Davidson method by blocking. *SIAM J. Sci. Comp.* 37, 6 (2015), 206–239. <https://doi.org/10.1137/140976017>
  - [33] Yousef Saad. 2006. Filtered Conjugate Residual-type Algorithms with Applications. *SIAM J. Matrix Anal. Appl.* 28, 3 (2006), 845–870. <https://doi.org/10.1137/060648945> arXiv:<https://doi.org/10.1137/060648945>
  - [34] Yousef Saad. 2011. *Numerical Methods for Large Eigenvalue Problems* (revised ed.). Classics in Applied Mathematics, Vol. 66. Society for Industrial and Applied Mathematics (SIAM), Philadelphia.
  - [35] Olaf Schenk, Matthias Bollhöfer, and Rudolf A. Römer. 2008. On Large-Scale Diagonalization Techniques for the Anderson Model of Localization. *SIAM Rev.* 50 (2008), 91–112.
  - [36] Sebastian Scherg, Thomas Kohlert, Pablo Sala, Frank Pollmann, Bharath Hebhe Madhusudhana, Immanuel Bloch, and Monika Aidelsburger. 2021. Observing non-ergodicity due to kinetic constraints in tilted Fermi-Hubbard chains. *Nature Communications* 12 (2021), 4490. <https://doi.org/10.1038/s41467-021-24726-0>
  - [37] Michael Schreiber, Sean S. Hodgman, Pranjal Bordia, Henrik P. Lüschen, Mark H. Fischer, Ronen Vosk, Ehud Altman, Ulrich Schneider, and Immanuel Bloch. 2015. Observation of many-body localization of interacting fermions in a quasirandom optical lattice. *Science* 349, 6250 (2015), 842–845. <https://doi.org/10.1126/science.aaa7432> arXiv:<https://www.science.org/doi/pdf/10.1126/science.aaa7432>
  - [38] Piotr Sierant, Maciej Lewenstein, and Jakub Zakrzewski. 2020. Polynomially Filtered Exact Diagonalization Approach to Many-Body Localization. *Phys. Rev. Lett.* 125 (Oct 2020), 156601. Issue 15. <https://doi.org/10.1103/PhysRevLett.125.156601>
  - [39] Gerard L. G. Sleijpen and Henk A. van der Vorst. 1996. A Jacobi-Davidson iteration method for linear eigenvalue problems. *SIAM J. Matrix Anal. Appl.* 17 (1996), 401–425.

- [40] Danny C. Sorensen. 2002. Numerical methods for large eigenvalues problems. *Acta Numerica* 11 (2002), 519–584.
- [41] A. Stathopoulos and K. Wu. 2002. A block orthogonalization procedure with constant synchronization requirements. *SIAM J. Sci. Comp.* 23 (2002), 2165–2182. Issue 6.
- [42] The Trilinos Project Team. 2020. The Trilinos Project Website. <https://trilinos.github.io> Accessed: 2022-03-17.
- [43] Alexander Weiße, Gerhard Wellein, Andreas Alvermann, and Holger Fehske. 2006. The kernel polynomial method. *Rev. Mod. Phys.* 78 (2006), 275–306.
- [44] Jan Winkelmann, Paul Springer, and Edoardo Di Napoli. 2019. ChASE: Chebyshev Accelerated Subspace Iteration Eigensolver for Sequences of Hermitian Eigenvalue Problems. *ACM Trans. Math. Softw.* 45, 2, Article 21 (apr 2019), 34 pages. <https://doi.org/10.1145/3313828>
- [45] Yunkai Zhou, Yousef Saad, Murilo L. Tiago, and James R. Chelikowsky. 2006. Self-consistent-field calculations using Chebychev-filtered subspace iteration. *J. Comp. Phys.* 219 (2006), 172–184.